LETTER

Valley-selective topologically ordered states in irradiated bilayer graphene

2D Materials

LETTER

Valley-selective topologically ordered states in irradiated bilayer graphene

RECEIVED
3 August 2017

REVISED
11 October 2017

ACCEPTED FOR PUBLICATION
18 October 2017

PUBLISHED
6 November 2017

Chunlei Qu, Chuanwei Zhang and Fan Zhang[1]

Department of Physics, University of Texas at Dallas, Richardson, TX 75080, United States of America

[1] Author to whom any correspondence should be addressed.

E-mail: zhang@utdallas.edu **(Fan Zhang)**

Keywords: bilayer graphene, Floquet physics, valley Hall, anomalous Hall, spin Hall, quantum Hall

Abstract

Gapless bilayer graphene is susceptible to a variety of spontaneously gapped states. As predicted by theory and observed by experiment, the ground state is, however, topologically trivial, because a valley-independent gap is energetically favorable. Here, we show that under the application of interlayer electric field and circularly polarized light, one valley can be selected to exhibit the original interaction instability while the other is frozen out. Tuning this Floquet system stabilizes multiple competing topologically ordered states, distinguishable by edge transport and circular dichroism. Notably, quantized charge, spin, and valley Hall conductivities coexist in one stabilized state.

1. Introduction

Chirally stacked few-layer graphene, ranging from the Bernal bilayer to its thicker cousins with Rhombohedral stacking, has become a paradigmatic platform for studying fascinating two-dimensional electron physics [1–4]. Unlike the linear Dirac bands in monolayer graphene, the bands in an N-layer system exhibit flatter dispersions $\sim\pm k^N$. Notably, the Fermi surface only consists of band touching points at two inequivalent hexagonal Brillouin zone corners, known as K and K' valleys. Intriguingly, the Fermi points are protected by the quantized Berry phases $\pm N\pi$ in the presence of a chiral symmetry between the two sublattices located at the top and bottom layers. This unique feature leads to band gap opening when an interlayer electric field breaks the chiral symmetry [5–10]. More remarkably, due to the large density-of-states near the Fermi points, the $N>1$ systems are susceptible to a variety of broken chiral symmetry states [11], in which each spin-valley flavor spontaneously transfers charge between layers to yield opening of quasiparticle energy gaps [12–15] and spreading of momentum-space Berry curvature [3].

The order competing is enriched by the $\mathcal{SU}(4)$ spin-valley symmetry [11–44]. The nearly-degenerate ground states can be topologically classified based on the signs of spontaneous gaps at each spin-valley [3, 18], analogous to those single-particle states in Haldane and Kane-Mele models [45, 46]. The intervalley exchange interactions, although extremely weak and often negligible, energetically favor those candidates with valley degeneracy [19], i.e. the same layer polarization at the two valleys. In order to minimize the electrostatic energy, hence the two spin flavors must polarize toward opposite layers . These two facts yield a topologically trivial layer-antiferromagnetic (LAF) ground state [3, 19, 20, 29], as recently confirmed by experiment [37–41].

One may naturally wonder whether and how the more exotic topologically ordered states [3, 18] can be stabilized. The key is to relax the aforementioned valley degeneracy; a possible route is to explicitly break both time reversal ($\mathcal{T}$) and spatial inversion ($\mathcal{P}$) symmetries that dictate the valley degeneracy. We find that under the application of interlayer electric field and circularly polarized light in bilayer graphene, one valley can be selected to exhibit the original $\pm k^N$-band touching [3] and weak interaction instability [12–15], whereas the other valley is frozen out due to a large field-induced gap, as illustrated in figure 1. When the interaction-driven gap at the selected valley is opposite to the field-induced gap at the frozen valley, the ground state is a quantum anomalous Hall (QAH) state.

Remarkably, when the selected-valley gaps become opposite between the two spin flavors, quantized charge, spin, and valley Hall conductivities coexist. As we will examine, such an exotic ordered state dubbed 'ALL' hereafter, elusive in the absence of the delicately applied fields or the electron-electron interactions, can be stabilized by tuning the interacting Floquet system, and different ordered states can be distinguished by edge transport and circular dichroism. We note that a light-irradiated Floquet state has been observed on

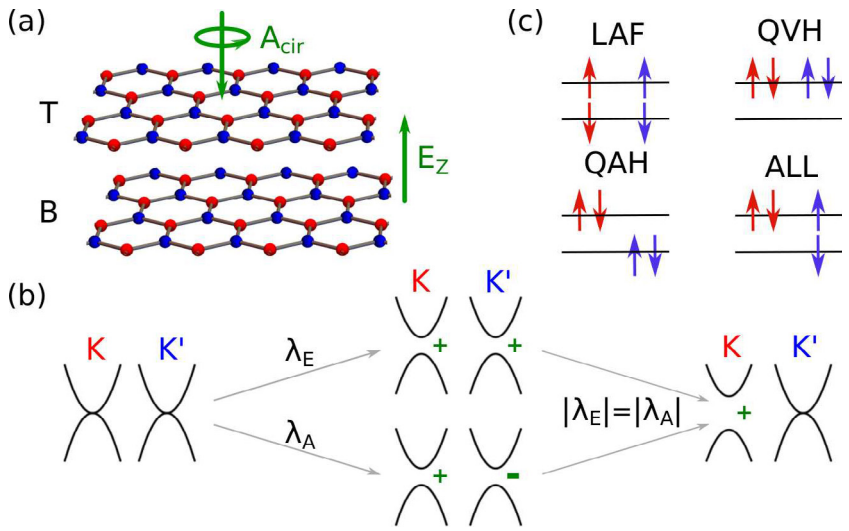

Figure 1. (a) Sketch of bilayer graphene under the application of an interlayer electric field and a circularly polarized light. (b) The electric (light) field opens an energy gap with the same (opposite) sign(s) at the two valleys. If both fields generate equal gap magnitudes, the energy gap of a selected valley vanishes. (c) Illustration of the layer polarizations in the four competing ordered states. The up/down arrows denote the two spins; the red/blue colors denote the two valleys.

a topological insulator (TI) surface [47, 48], and our predicted ordered Floquet states may be similarly studied in chiral graphene experiments [33–44].

2. Floquet theory

We first establish our notation by discussing the effective Hamiltonian [3] that can coherently describe graphene ($N = 1$), its Bernal bilayer ($N = 2$), and its Rhombohedral few-layers ($N > 2$), to which our main results derived for the bilayer system can be generalized. Such a model reads

$$h_N = \frac{(v_0\hbar k)^N}{(-\gamma_1)^{N-1}}[\cos(N\phi_{\boldsymbol{k}})\sigma_x + \sin(N\phi_{\boldsymbol{k}})\sigma_y] + \lambda\sigma_z, \tag{1}$$

where v_0 is the Fermi velocity of graphene, $\cot\phi_{\boldsymbol{k}} = \tau k_x/k_y$, and $\tau = \pm$ label the K and K' valleys. $\gamma_1 \sim 0.4$ eV is the interlayer nearest-neighbor hopping energy, which sets the largest energy scale of the model. The Pauli matrices $\boldsymbol{\sigma}$ act on the layer-pseudospin space spanned by the two sublattices relevant at low energy, i.e. the top A and bottom B without interlayer nearest neighbors. For $\lambda = 0$, the gapless spectrum of h_N has two band touch points at K and K', protected by the chiral ($\mathcal{C}$) symmetry between the two sublattices.

$\lambda\sigma_z$ is a mass term that characterizes $\mathcal{C}$ symmetry breaking and hence opens an energy gap whenever $\lambda \neq 0$. It turns out that the mass term can be explicitly induced by an interlayer electric field or a circularly polarized light, or spontaneously generated by electron-electron interactions. In the first scenario, as demonstrated by the experiments in $N > 1$ systems [5–10], the interlayer electric field E_z breaks $\mathcal{P}$ and $\mathcal{C}$ symmetries by producing

$$\lambda = \lambda_E = -eE_z d, \tag{2}$$

where d is the layer separation. λ_E is spin-valley independent, as required by $\mathcal{T}$ and spin $\mathcal{SU}(2)$ symmetries.

To demonstrate the second scenario, consider a circularly polarized light shining on a few-layer. This amounts to applying a time-dependent electromagnetic gauge potential $\boldsymbol{A}(t) = A_0(\xi\sin\omega t, \cos\omega t)$ to the system, where $\xi = \pm$ denote the light helicities. In Floquet theory, such a periodically driven system can effectively be described by a static Hamiltonian [49, 50]

$$h_{\rm eff} = h_0 + \frac{1}{\hbar\omega}\sum_{j=1}^{\infty}\frac{1}{j}[\mathcal{V}_{+j}, \mathcal{V}_{-j}] + \mathcal{O}\left(\frac{1}{\omega^2}\right). \tag{3}$$

h_0 is the time-independent Hamiltonian without the periodic drive; $\mathcal{V}_{\pm j} = (\omega/2\pi)\int \mathcal{V}(t)e^{\mp ij\omega t}dt$ are the Fourier components of the time-dependent periodic potential $\mathcal{V}(t)$. Similarly to how equation (2) was derived [51], we apply $\boldsymbol{A}(t)$ to the original full-band model of N-layer graphene, followed by a projection to the two-band model at low energy. In the *high-frequency* limit, to the leading order the circularly polarized light yields

$$\lambda = \lambda_A\tau = \frac{e^2v_0^2A_0^2}{\hbar\omega}\xi\tau. \tag{4}$$

The radiation field can yield a mass term λ_A as its definite helicity breaks $\mathcal{T}$ and $\mathcal{C}$ symmetries. The intact spin $\mathcal{SU}(2)$ and $\mathcal{P}$ symmetries dictate λ_A to be spin independent but opposite at the two valleys. λ_A was originally derived in the seminal work on radiated monolayer graphene [52–55], and a similar gap has been experimentally observed on the TI surface [47, 48]. Here we generalize the idea to graphene few-layers and demonstrate the general validity of equation (4).

In a many-body scenario, Coulomb interactions can generate masses in the quasiparticle spectra of $N>1$ systems [3]. While a microscopic theory will be given later, the ground state turns out to be LAF [38–43], breaking all the symmetries. The two spin flavors are polarized to opposite layers spontaneously as if they are subjected to opposite λ_E mean-fields, i.e. $\lambda \propto s_z$ in equation (1).

In each scenario, the mass generation in equation (1) spreads the Berry curvature, which is integrated to $N\mathrm{sgn}(\lambda)\tau/2$ for each spin-valley [3]. Hence, λ_A induces a QAH state with Chern number $2N$, which is reminiscent of the Haldane model [45]; λ_E produces a quantum valley Hall (QVH) state since the valley Chern numbers are opposite for different valleys [3, 56–61], analogous to the quantum spin Hall state [46]. Metallic in-gap states have indeed been experimentally observed [62–65] along a QVH domain wall in bilayer graphene where the edge conductance appears to approach $4e^2/h$. By contrast, the LAF state is topologically trivial since it can be viewed as two opposite copies of QVH states. As motivated in *Introduction* and illustrated in figure 1(b), when $|\lambda_A|=|\lambda_E|$, one valley can be selected to exhibit the original $\pm k^N$-band touching, whereas the other valley is almost frozen out due to a large field-induced gap. The interactions generate masses at the selected valley, whose signs determine three competing ordered states: QAH, QVH, and the emergent ALL states. With masses opposite (the same) in sign for the two spins at the selected (frozen) valley, the ALL state can be viewed as a QVH state for one spin but QAH for the other. Remarkably, such a state breaks all the symmetries and exhibits charge, spin, and valley Chern numbers of N. More remarkably, the ALL state is a synergistic consequence of intrinsic interactions and external fields, instead of due to any magnetic moment or spin-orbit coupling.

3. Hartree–Fock theory and phase diagram

We now study the phase diagram enrichment in terms of the following ordered state quasiparticle Hamiltonian [3, 38, 39]:

$$\mathcal{H}^{\mathrm{HF}} = \sum_{\boldsymbol{k}\alpha\beta s\tau} c^{\dagger}_{\boldsymbol{k}\alpha s\tau}[h_N + h_H + h_F + h_V]c_{\boldsymbol{k}\beta s\tau}, \tag{5a}$$

$$h_{\mathrm{H}} = [V_0\Delta_0\delta^{\alpha\beta} + V_z\Delta_z\sigma_z^{\alpha\beta}], \tag{5b}$$

$$h_{\mathrm{F}} = -[V_0 + V_z\sigma_z^{\alpha\alpha}\sigma_z^{\beta\beta}]\Delta^{s\tau}_{\alpha\beta}, \tag{5c}$$

$$h_{\mathrm{V}} = -[V'_0 + V'_z\sigma_z^{\alpha\alpha}\sigma_z^{\beta\beta}]\Delta^{s\bar{\tau}}_{\alpha\beta}, \tag{5d}$$

which has well reproduced the experimentally observed gap size and T_c in bilayer graphene. In equation (5), Greek letters label layer, s labels spin, and τ labels valley. $V_{0,z}=(V_s\pm V_d)/2$ denotes the average (difference) of intralayer and interlayer interactions at the same valley, and likewise $V'_{0,z}=(V'_s\pm V'_d)/2$ for valley-exchange interactions [19]. The density matrix $\Delta^{s\tau}_{\alpha\beta}=\sum_{\boldsymbol{k}}\langle c^{\dagger}_{\boldsymbol{k}\alpha s\tau}c_{\boldsymbol{k}\beta s\tau}\rangle_f/A$ must be determined self-consistently. We introduce $\Delta^{s\tau}_{0,z}$ as the density sum (difference) of the top and bottom layers for one spin-valley flavor and $\Delta_{0,z}=\sum_{s\tau}\Delta^{s\tau}_{0,z}$ as the total density sum (difference). The mean-field interaction vertices must be diagonal in layer due to in-plane rotational symmetry; neither spin nor valley coherence can be established spontaneously since the long-range Coulomb interactions $V_{0,z}$ dominate. Therefore, in equation (1) λ reads

$$\lambda^{s\tau} = \lambda_E + \lambda_A\tau + V_z\Delta_z - \frac{V_s}{2}\Delta_z^{s\tau} - \frac{V'_s}{2}\Delta_z^{s\bar{\tau}}, \tag{6}$$

where $\Delta_z^{s\tau}$ minimize the energy density functional

$$\varepsilon_g = -\frac{1}{A}\sum_{\boldsymbol{k}s\tau}\sqrt{(\lambda^{s\tau})^2 + (v_0\hbar k)^{2N}/\gamma_1^{2N-2}} - \left[\frac{V_z}{2}(\Delta_z)^2 - \frac{V_s}{4}\sum_{s\tau}(\Delta_z^{s\tau})^2 - \frac{V'_s}{4}\sum_{s\tau}\Delta_z^{s\tau}\Delta_z^{s\bar{\tau}}\right]. \tag{7}$$

Given that the subtracted in the second line of equation (7) is exactly half of the mean-field interactions that are implicit in the first line, the three interaction parameters ($V_s \gg V_z, V'_s > 0$) play different roles in order competing. The intralayer exchange V_s causes spontaneous layer polarization in each spin-valley, whereas the Hartree energy determined by V_z prevents any total layer polarization. Although rather weak, the valley-exchange interaction V'_s favors a ground state in which different valleys have the same layer polarization. Therefore, for $E_z = A_0 = 0$, the ground state must be the LAF state in which different spin (valley) flavors are layer polarized in the opposite (same) sense, as observed in experiment [38–43].

We now examine how the circularly polarized radiation enriches the order competing and stabilizes the ordered QAH and ALL states. We focus on the $N=2$ case to facilitate our numerics; the qualitative results should apply to $N>2$ cases. Figure 2(a) shows the phase diagram, which exhibits four competing orders and mirror symmetries with respect to $\lambda_{E,A}=0$ lines. The LAF state exists in the limit of vanishing external fields. A sufficiently large λ_E (λ_A) favors the QVH (QAH) state. Near the $|\lambda_E|=|\lambda_A|$ line, there emerges the ALL state.

In the phase diagram figure 2(a), the positions of the critical points A–D are determined by the strengths of three interaction parameters. This has also been discussed in the above analysis of equations (6) and (7). (i) The experimental LAF gap is about 2 meV at zero fields [38, 39]; it follows from equations (6) and (7) that the dominating intralayer exchange $\nu_0 V_s = 0.2992$, where ν_0 is the density of states per flavor. (ii) Although both QAH and LAF states are ordered without total layer polarization, it is the weak valley-exchange interaction V'_s that favors the LAF state [19], in which different valleys have the same layer polarization. Consequently, the A point shifts toward a larger λ_A if V'_s/V_s is stronger, as shown in figure 2(c). (iii) The weak Hartree

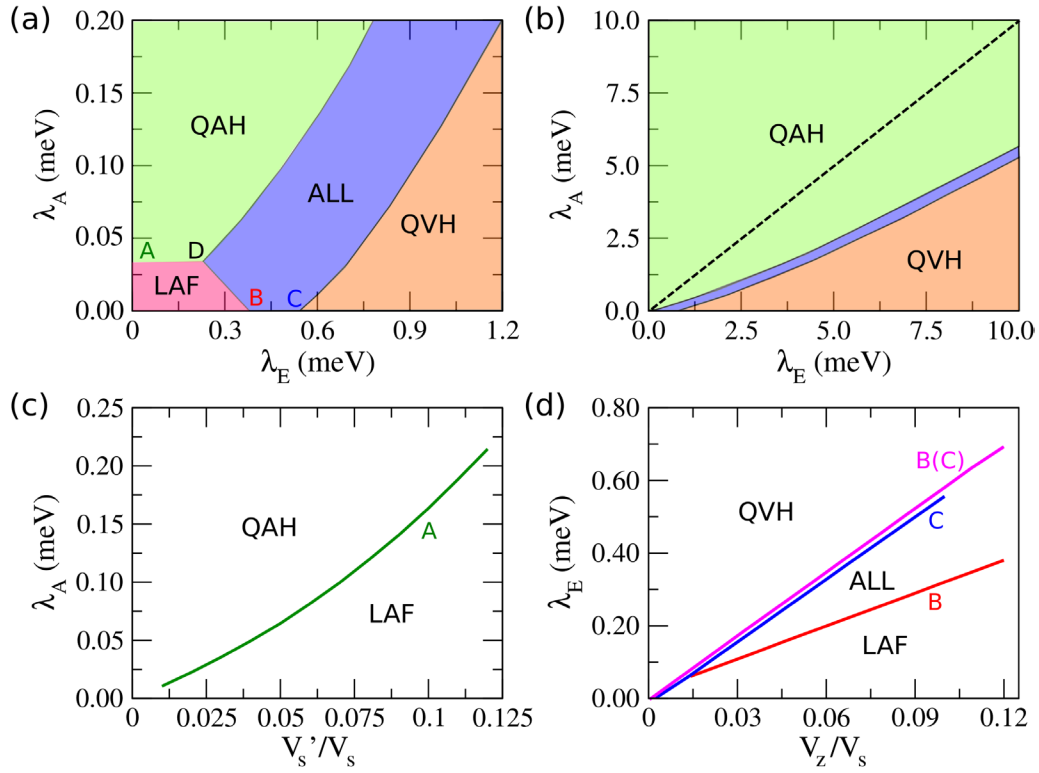

Figure 2. ((a) and (b)) Phase diagram of bilayer graphene at small and large fields, respectively. The Hartree interaction $V_z = 0.1V_s$; the valley-exchange interaction $V_s' = 0.03V_s$. ((c)–(d)) The dependences of the critical points A–C in (a) on V_s' and on V_z, respectively. The red and blue lines are for $V_s' = 0.02V_s$, and the purple line is for $V_s' = 0.08V_s$.

interaction V_z prevents any total layer polarization induced by finite λ_E. Thus, both B and C shift toward larger λ_E's if V_z/V_s is stronger, as shown in figure 2(d). (iv) Interactions favor the QAH state over the QVH state and produces the novel ALL state near their transition. The ALL-state phase boundaries in figure 2(b) are shifted away from the $|\lambda_E| = |\lambda_A|$ line, which separates the QAH and QVH states in the absence of interactions. Such a shift arises from the compensation of the Hartree energy by the λ_E mass in the frozen valley τ, and it is given by $|\lambda_E| - |\lambda_A| \sim V_z|\Delta_z^{\tau}|$. The width of the ALL-state regime is similarly determined, but by the selected valley $\bar{\tau}$, and it is given by $\delta|\lambda_E| \sim V_z|\Delta_z^{\bar{\tau}}|$. Note that since B is sensitive to the change of V_s' whereas C is not, the ALL state may disappear at $\lambda_A = 0$ if V_s' exceeds a critical value, as exemplified by the magenta line in figure 2(d). (Here we predict that a circularly polarized light can stabilize and control the ALL state without Landau levels. Its quantum Hall ferromagnetic variant has been experimentally observed at $\nu = 2$ [42].)

The parameters for the emergence of the intriguing ALL state in the phase diagram figure 2(b) can be fitted to $\lambda_A \approx 0.6\lambda_E - 1$ meV at relatively large fields. To observe the ALL state, e.g. one can scan the parameter region around $\lambda_E \sim 10$ meV and $\lambda_A \sim 5$ meV. Given equation (2), the electric field strength is $E_z = \lambda_E/(ed) \sim 30$ mV/nm where $d = 3.4$ Å is the interlayer separation. The laser frequency, which should be much larger than the interaction-driven or field-induced energy gap ~10 meV but much smaller than $\gamma_1 \sim 0.4$ eV, can be chosen as $\hbar\omega \sim 100$ meV. This corresponds to a light frequency ~25 THz or a light wavelength ~12 μm. Given equation (4), we can obtain the energy flux of the light is $I = \omega^2 A_0^2/\mu_0 c \sim 3 \times 10^{10}\,\mathrm{W\,m^{-2}}$.

4. Circular dichroism

In addition to the number of valley-projected chiral edge states (figures 3(d) and (e)) dictated by the aforementioned Chern numbers, different topologically ordered states may also be characterized by optical means. Here we consider *terahertz* absorbance [66, 67] and its dichroism [68–71] using a *second*, circularly polarized, normally incident light. Consider a *weak* probe beam $\boldsymbol{A}' = A_0'(\xi' \sin\omega' t, \cos\omega' t)$, and to the first order the induced perturbation reads

$$\mathcal{V}' = \frac{ie\hbar v_0^2 A_0'}{\gamma_1}(\tau k_x - ik_y)(\sigma_x + i\sigma_y)e^{i\xi'\tau\omega' t} + \text{h.c.}. \tag{8}$$

Using Fermi's golden rule, we obtain the interband transition probability, followed by the flavor absorbance

$$P_{\xi'}^{s\tau} = \frac{\pi\alpha}{2}\left(1 + \xi'\tau\frac{2\lambda^{s\tau}}{\hbar\omega'}\right)^2 \Theta(\hbar\omega' - 2|\lambda^{s\tau}|), \tag{9}$$

where α is the fine structure constant. We further define the total absorbance and the circular dichroism as

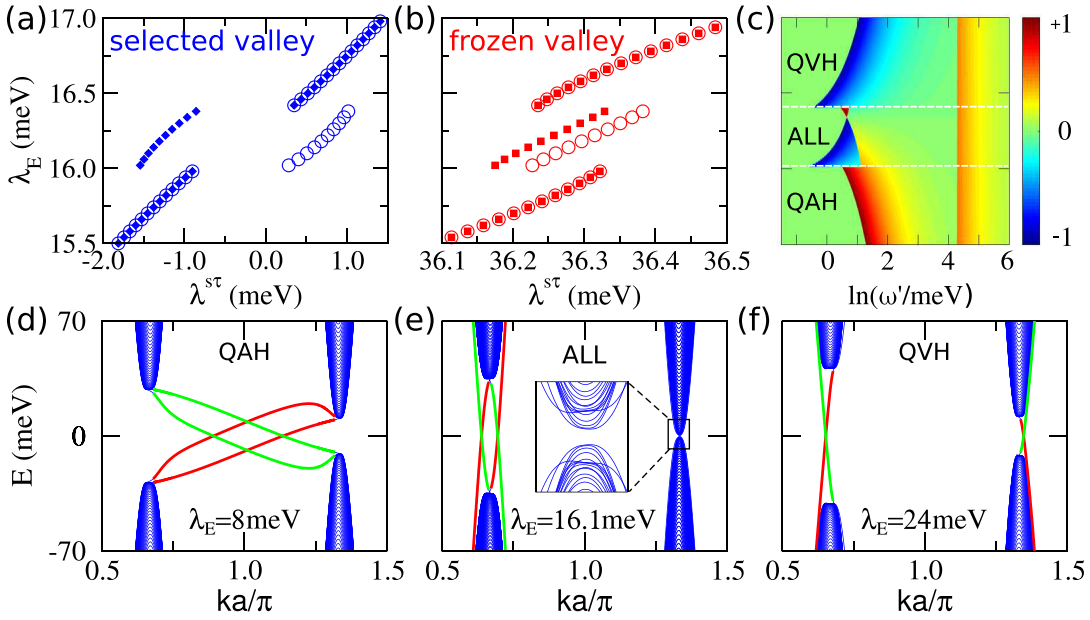

Figure 3. ((a) and (b)) Ordered state masses $\lambda^{s\tau}$ and (c) circular dichroism $\eta(\omega')$ of bilayer graphene, as functions of λ_E. The square and circle denote different spins, λ_A is fixed at 10 meV, and other parameter values are the same as in figure 2(b). ((d)–(f)) Protected zigzag edge states for the three phases. The red and green states, spin degenerate in (d) and (f) but non degenerate in (e), localize at opposite edges. Note that a zigzag edge is the best to observe the charateristic edge states but not required. The edge states are robust as long as the two valleys are well separated in the edge Brillouin zone and the boundary (or domain wall) is smooth in a scale much larger than the inverse of the separation.

$$P_{\xi'} = \sum_{s\tau} P^{s\tau}_{\xi'} \quad \text{and} \quad \eta = \frac{P_+ - P_-}{P_+ + P_-}. \qquad (10)$$

In the limit of $\hbar\omega' \gg |\lambda|$ or $\lambda \to 0$, the total absorbance recovers the universal result $2\pi\alpha$, independent of the light helicity or polarization. This results in $\eta \to 0$. Close to the thresholds, $\hbar\omega' = 2|\lambda^{s\tau}|$, a circularly polarized light is either destructively blocked or constructively absorbed, depending on the light helicity, the valley index, and the mass sign. This leads to sharp peaks in η.

Figure 3 plots $\lambda^{s\tau}$ and $\eta(\omega')$ as functions of λ_E for the case of $\lambda_A = 10$ meV. As the electric field increases, the ground state undergoes QAH-ALL-QVH transitions. At the frozen valley the masses are large and of uniform sign for the two spins, whereas at the selected valley the masses are small and relatively inverted for zero, one, and two spin flavors, respectively, in QVH, ALL, and QAH states. Universally, η shows a marked jump when the selected valley starts to be probed and gradually falls upon increasing ω', except that η switches sign for the ALL state due to the different magnitudes of λ^s. Distinctively, when the frozen valley starts to be probed, η exhibits a tiny jump for the QAH and ALL states but switches sign for the QVH state and progressively vanishes with further advancing ω'. By contrast, the LAF state exhibits little circular dichroism, because the two spin flavors have opposite masses $\sim$2 meV.

5. Discussion

The absorption spectroscopy (or optical conductivity) and circular dichroism provides efficient means not only to measure the flavor dependent mass $\lambda^{s\tau}$ but also to distinguish the competing ordered states. It follows that the photoluminescence can also be circularly and valley polarized, controllable by the external fields. Similarly, opto-valley, -spin, and -charge Hall effects may be feasible upon the pumping of these fields, given the nontrivial conduction-band Berry curvature [3].

Three comments are in order. (i) Graphene does not reflect a significant amount of light as opposed to TI's, and the interaction effects are more pronounced in suspended samples. Transmission spectroscopy is thus suggested to study the predicted effects. (ii) In non-equilibrium periodically driven systems, interactions and band populations are important and delicate issues for Floquet states [50, 72, 73]. In our case, additional terms beyond equation (4) produced by interactions can be safely ignored, as we focus on the *weak* interaction instability implied by peculiar band structures. Given the fact that absorbance per graphene layer is only $\pi\alpha \sim 2.3\%$ [66, 67], presumably the band population is almost intact in the presence of the high-frequency light. (iii) Our Hartree–Fock theory only captures the most essential physics of Floquet bilayer graphene. The weak yet important interaction parameters V_z and V_s' may vary from case to case and should be determined by future experiments. The phase boundaries in figure 2 are likely to be quantitatively modified by the thermal proliferation of domain walls separating different ordered states [31].

At single-particle level, the Floquet idea [52–55] was theoretically applied to TI's [74] and semimetals [75–77], and experimentally realized in photonic crystals [78], TI surfaces [47, 48], and ultracold atoms [79]. Our proposal paves the way for generalizing the idea to

a paradigmatic many-body system (i.e. chiral few-layer graphene), and revealed the significant roles played by interactions in stabilizing topologically ordered states (e.g. the ALL state) hardly accessible at single-particle level.

Acknowledgments

This work is supported by NSF (PHY-1505496), ARO (W911NF-17-1-0128), AFOSR (FA9550-16-1-0387), and UTD Research Enhancement Funds.

ORCID iDs

Chunlei Qu https://orcid.org/0000-0002-3080-8698
Fan Zhang https://orcid.org/0000-0003-4623-4200

References

[1] Neto A H C, Guinea F, Peres N M R, Novoselov K S and Geim A K 2009 The electronic properties of graphene *Rev. Mod. Phys.* **81** 109
[2] Min H and MacDonald A H 2008 Electronic structure of multilayer graphene *Prog. Theor. Phys. Suppl.* **176** 227
[3] Zhang F, Jung J, Fiete G A, Niu Q and MacDonald A H 2011 Spontaneous quantum Hall states in chirally stacked few-layer graphene systems *Phys. Rev. Lett.* **106** 156801
[4] Ren Y, Qiao Z and Niu Q 2016 Topological phases in two-dimensional materials: a review *Rep. Prog. Phys.* **79** 066501
[5] McCann E and Fal'ko V I 2006 Landau-level degeneracy and quantum Hall effect in a graphite bilayer *Phys. Rev. Lett.* **96** 086805
[6] Ohta T, Bostwick A, Seyller T, Horn K and Rotenberg E 2006 Controlling the electronic structure of bilayer graphene *Science* **313** 951
[7] Zhang Y, Tang T-T, Girit C, Hao Z, Martin M C, Zettl A, Crommie M F, Shen Y R and Wang F 2009 Direct observation of a widely tunable bandgap in bilayer graphene *Nature* **459** 820
[8] Mak K F, Lui C H, Shan J and Heinz T F 2009 Observation of an electric-field-induced band gap in bilayer graphene by infrared spectroscopy *Phys. Rev. Lett.* **102** 256405
[9] Lui C H, Li Z, Mak K F, Cappelluti E and Heinz T F 2011 Observation of an electrically tunable band gap in trilayer graphene *Nat. Phys.* **7** 944
[10] Zou K, Zhang F, Clapp C, MacDonald A H and Zhu J 2013 Transport studies of dual-gated ABC and ABA trilayer graphene: band gap opening and band structure tuning in very large perpendicular electric fields *Nano Lett.* **13** 369
[11] Zhang F 2015 Spontaneous chiral symmetry breaking in bilayer graphene *Synth. Met.* **210** 9
[12] Min H, Borghi G, Polini M and MacDonald A H 2008 Pseudospin magnetism in graphene *Phys. Rev.* B **77** 041407
[13] Sun K, Yao H, Fradkin E and Kivelson S A 2009 Topological insulators and nematic phases from spontaneous symmetry breaking in 2D Fermi systems with a quadratic band crossing *Phys. Rev. Lett.* **103** 046811
[14] Zhang F, Min H, Polini M and MacDonald A H 2010 Spontaneous inversion symmetry breaking in graphene bilayers *Phys. Rev.* B **81** 041402
[15] Nandkishore R and Levitov L 2010 Dynamical screening and exotic instability in bilayer graphene *Phys. Rev. Lett.* **104** 156803
[16] Vafek O and Yang K 2010 Many-body instability of Coulomb interacting bilayer graphene: renormalization group approach *Phys. Rev.* B **81** 041401
[17] Lemonik Y, Aleiner I L, Toke C and Fal'ko V I 2010 Spontaneous symmetry breaking and Lifshitz transition in bilayer graphene *Phys. Rev.* B **82** 201408
[18] Nandkishore R and Levitov L 2010 Quantum anomalous Hall state in bilayer graphene *Phys. Rev.* B **82** 115124
[19] Jung J, Zhang F and MacDonald A H 2011 Lattice theory of pseudospin ferromagnetism in bilayer graphene: competing interaction-induced quantum Hall states *Phys. Rev.* B **83** 115408
[20] Zhang F and MacDonald A H 2012 Distinguishing spontaneous quantum Hall states in bilayer graphene *Phys. Rev. Lett.* **108** 186804
[21] Trushin M and Schliemann J 2012 Polarization-sensitive absorption of THz radiation by interacting electrons in chirally stacked multilayer graphene *New. J. Phys.* **14** 095005
[22] Lang T C, Meng Z Y, Scherer M M, Uebelacker S, Assaad F F, Muramatsu A, Honerkamp C and Wessel S 2012 Antiferromagnetism in the Hubbard model on the Bernal-stacked honeycomb bilayer *Phys. Rev. Lett.* **109** 126402
[23] Scherer M M, Uebelacker S and Honerkamp C 2012 Instabilities of interacting electrons on the honeycomb bilayer *Phys. Rev.* B **85** 235408
[24] Lemonik Y, Aleiner I and Fal'ko V I 2012 Competing nematic, antiferromagnetic, and spin-flux orders in the ground state of bilayer graphene *Phys. Rev.* B **85** 245451
[25] Cvetkovic V, Throckmorton R E and Vafek O 2012 Electronic multicriticality in bilayer graphene *Phys. Rev.* B **86** 075467
[26] Yan X-Z and Ting C S 2012 Absence of gapped broken inversion symmetry phase of electrons in bilayer graphene under the renormalized ring-diagram approximation *Phys. Rev.* B **86** 125438
Yan X-Z and Ting C S 2012 Possible broken inversion and time-reversal symmetry state of electrons in bilayer graphene *Phys. Rev.* B **86** 235126
Yan X-Z and Ting C S 2013 Ordered-current state of electrons in bilayer graphene *Phys. Rev.* B **88** 045410
[27] Gorbar E V, Gusynin V P, Miransky V A and Shovkovy I A 2012 Coexistence and competition of nematic and gapped states in bilayer graphene *Phys. Rev.* B **86** 125439
[28] Zhang F, Min H and MacDonald A H 2012 Competing ordered states in bilayer graphene *Phys. Rev.* B **86** 155128
[29] Kharitonov M 2012 Antiferromagnetic state in bilayer graphene *Phys. Rev.* B **86** 195435
[30] Zhu L, Aji V and Varma C M 2013 Ordered loop current states in bilayer graphene *Phys. Rev.* B **87** 035427
[31] Li X, Zhang F, Niu Q and MacDonald A H 2014 Spontaneous layer-pseudospin domain walls in bilayer graphene *Phys. Rev. Lett.* **113** 116803
[32] Zhang J, Nandkishore R and Rossi E 2015 Disorder-tuned selection of order in bilayer graphene *Phys. Rev.* B. **91** 205425
[33] Martin J, Feldman B E, Weitz R T, Allen M T and Yacoby A 2010 Local compressibility measurements of correlated states in suspended bilayer graphene *Phys. Rev. Lett.* **105** 256806
[34] Weitz R T, Allen M T, Feldman B E, Martin J and Yacoby A 2010 Broken-symmetry states in doubly gated suspended bilayer graphene *Science* **330** 812
[35] Mayorov A S *et al* 2011 Interaction-driven spectrum reconstruction in bilayer graphene *Science* **333**, 860
[36] Bao W *et al* 2011 Stacking-dependent band gap and quantum transport in trilayer graphene *Nat. Phys.* **7** 948
[37] Freitag F, Trbovic J, Weiss M and Schönenberger C 2012 Spontaneously gapped ground state in suspended bilayer graphene *Phys. Rev. Lett.* **108** 076602
[38] Velasco J Jr *et al* 2012 Transport spectroscopy of symmetry-broken insulating states in bilayer graphene *Nat. Nanotechnol.* **7** 156
[39] Bao W, Velasco J Jr, Zhang F, Jing L, Standley B, Smirnov D, Bockrath M, MacDonald A H and Lau C N 2012 Evidence for a spontaneous gapped state in ultraclean bilayer graphene *Proc. Natl Acad. Sci. USA* **109** 10802
[40] Veligura A, van Elferen H J, Tombros N, Maan J C, Zeitler U and van Wees B J 2012 Transport gap in suspended bilayer graphene at zero magnetic field *Phys. Rev.* B **85** 155412
[41] Freitag F, Weiss M, Maurand R, Trbovic J and Schönenberger C 2013 Spin symmetry of the bilayer graphene ground state *Phys. Rev.* B **87** 161402

[42] Velasco J Jr, Lee Y, Zhang F, Myhro K, Tran D, Deo M, Smirnov D, MacDonald A H and Lau C N 2014 Competing ordered states with filling factor two in bilayer graphene *Nat. Commun.* **5** 4550
[43] Lee Y, Tran D, Myhro K, Velasco J Jr, Gillgren N, Lau C N, Barlas Y, Poumirol J M, Smirnov D and Guinea F 2014 Competition between spontaneous symmetry breaking and single-particle gaps in trilayer graphene *Nat. Commun.* **5** 5656
[44] Grushina A L, Ki D-K, Koshino M, Nicolet A A L, Faugeras C, McCann E, Potemski M and Morpurgo A F 2015 Insulating state in tetralayers reveals an even–odd interaction effect in multilayer graphene *Nat. Commun.* **6** 6419
[45] Haldane F D M 1988 Model for a quantum Hall effect without Landau levels: condensed-matter realization of the 'parity anomaly' *Phys. Rev. Lett.* **61** 2015
[46] Kane C L and Mele E J 2005 Quantum spin Hall effect in graphene *Phys. Rev. Lett.* **95** 226801
[47] Wang Y H, Steinberg H, Jarillo-Herrero P and Gedik N 2013 Observation of Floquet–Bloch states on the surface of a topological insulator *Science* **342** 453
[48] Fregoso B M, Wang Y H, Gedik N and Galitski V 2013 Driven electronic states at the surface of a topological insulator *Phys. Rev.* B **88** 155129
[49] Goldman N and Dalibard J 2014 Periodically driven quantum systems: effective Hamiltonians and engineered gauge fields *Phys. Rev.* X **4** 031027
[50] Bukov M, D'Alessio L and Polkovnikov A 2015 Universal high-frequency behavior of periodically driven systems: from dynamical stabilization to Floquet engineering *Adv. Phys.* **64** 139
[51] Zhang F, Sahu B, Min H and MacDonald A H 2010 Band structure of ABC-stacked graphene trilayers *Phys. Rev.* B **82** 035409
[52] Oka T and Aoki H 2009 Photovoltaic Hall effect in graphene *Phys. Rev.* B **79** 081406
[53] Kitagawa T, Berg E, Rudner M and Demler E 2010 Topological characterization of periodically driven quantum systems *Phys. Rev.* B **82** 235114
[54] Morell E S and Foa Torres L E F 2012 Radiation effects on the electronic properties of bilayer graphene *Phys. Rev.* B **86** 125449
[55] Perez-Piskunow P M, Usaj G, Balseiro C A and Foa Torres L E F 2014 Floquet chiral edge states in graphene *Phys. Rev.* B **89** 121401
[56] Martin I, Blanter Y M and Morpurgo A F 2008 Topological confinement in bilayer graphene *Phys. Rev. Lett.* **100** 036804
[57] Li J, Martin I, Büttiker M and Morpurgo A F 2011 Topological origin of subgap conductance in insulating bilayer graphene *Nat. Phys.* **7** 38
[58] Qiao Z, Jung J, Niu Q and MacDonald A H 2011 Electronic highways in bilayer graphene *Nano Lett.* **11** 3453
[59] Zarenia M, Pereira J M Jr, Farias G A and Peeters F M 2011 Chiral states in bilayer graphene: magnetic field dependence and gap opening *Phys. Rev.* B **84** 125451
[60] Zhang F, MacDonald A H and Mele E J 2013 Valley Chern numbers and boundary modes in gapped bilayer graphene *Proc. Natl Acad. Sci. USA* **110** 10546
[61] Vaezi A, Liang Y, Ngai D H, Yang L and Kim E-A 2013 Topological edge states at a tilt boundary in gated multilayer graphene *Phys. Rev.* X **3** 021018
[62] Ju L *et al* 2015 Topological valley transport at bilayer graphene domain walls *Nature* **520** 650
[63] Li J, Wang K, McFaul K J, Zern Z, Ren Y F, Watanabe K, Taniguchi T, Qiao Z H and Zhu J 2016 Gate-controlled topological conducting channels in bilayer graphene *Nat. Nanotechnol.* **11** 1060
[64] Yin L-J, Jiang H, Qiao J-B and He L 2016 Direct imaging of topological edge states at a bilayer graphene domain wall *Nat. Commun.* **7** 11760
[65] Jiang L *et al* 2016 Soliton-dependent plasmon reflection at bilayer graphene domain walls *Nat. Mater.* **15** 840
[66] Nair R R, Blake P, Grigorenko A N, Novoselov K S, Booth T J, Stauber T, Peres N M R and Geim A K 2008 Fine structure constant defines visual transparency of graphene *Science* **320** 1308
[67] Mak K F, Sfeir M Y, Wu Y, Lui C H, Misewich J A and Heinz T F 2008 *Phys. Rev. Lett.* **101** 196405
[68] Xu X, Yao W, Xiao D and Heinz T F 2014 Spin and pseudospins in layered transition metal dichalcogenides *Nat. Phys.* **10** 343
[69] Yao W, Xiao D and Niu Q 2008 Valley-dependent optoelectronics from inversion symmetry breaking *Phys. Rev.* B **77** 235406
[70] Trushin M and Schliemann J 2011 Pseudospin in optical and transport properties of graphene *Phys. Rev. Lett.* **107** 156801
[71] Pan H, Li X, Zhang F and Yang S A 2015 Perfect valley filter in a topological domain wall *Phys. Rev.* B **92** 041404
[72] D'Alessio L and Rigol M 2015 Dynamical preparation of Floquet Chern insulators *Nat. Commun.* **6** 8336
[73] Seetharam K I, Bardyn C-E, Lindner N H, Rudner M S and Refael G 2015 Controlled population of Floquet-Bloch state via coupling to Bose and Fermi baths *Phys. Rev.* X **5** 041050
[74] Lindner N H, Refael G and Galitski V 2011 Floquet topological insulator in semiconductor quantum wells *Nat. Phys.* **7** 490
[75] Ezawa M 2013 Photoinduced topological phase transition and a single Dirac-cone state in silicene *Phys. Rev. Lett.* **110** 026603
[76] Chan C, Lee P A, Burch K S, Han J H and Ran Y 2016 When chiral photons meet chiral fermions: photoinduced anomalous Hall effects in Weyl semimetals *Phys. Rev. Lett.* **116** 026805
[77] Yan Z and Wang Z 2016 Tunable Weyl semimetals in periodically driven nodal line semimetals *Phys. Rev. Lett.* **117** 087402
[78] Rechtsman M C, Zeuner J M, Plotnik Y, Lumer Y, Podolsky D, Dreisow F, Nolte S, Segev M and Szameit A 2013 Photonic Floquet topological insulators *Nature* **496** 196
[79] Jotzu G, Messer M, Desbuquois R, Lebrat M, Uehlinger T, Greif D and Esslinger T 2014 Experimental realization of the topological Haldane model with ultracold fermions *Nature* **515** 237